



# Effect of segmental compatibility imposed over metal based polybutadiene polyurethane

Moumita Dhara<sup>a</sup>, Nitai Giri<sup>a</sup>, B. Narasimha Rao<sup>a</sup>, A.K. Patra<sup>b</sup>, P.U. Sastry<sup>b</sup>, Mahesh Shrikishan Ingole<sup>c</sup>, Tushar Jana<sup>a,\*</sup>

<sup>a</sup> School of Chemistry, University of Hyderabad, Hyderabad 500046, India

<sup>b</sup> Solid State Physics Division, Bhabha Atomic Research Centre, Trombay, Mumbai 400085, India

<sup>c</sup> Department of Aerospace Engineering, Indian Institute of Technology Madras, Chennai 600036, India

## ARTICLE INFO

### Keywords:

Polyurethane  
Hydroxyl terminated polybutadiene  
Segmental mixing  
Burn rate modifier  
Ferrocene

## ABSTRACT

Series of metal based polyurethanes (PUs) have been synthesized from hydroxyl terminated polybutadiene (HTPB) with combination of a potential energetic material, 2,4-dinitrobenzene (DNB) and burn rate (BR) enhancer, ferrocene with two objectives: (1) exerting flexibility into otherwise brittle PU film and (2) increasing BR of composite solid propellant (CSP). HTPB was first functionalized with DNB at the terminal carbons and then ferrocene was grafted radically as poly (vinyl ferrocene) (PVF) chain onto the pendant vinyl bond of HTPB. The degree of PVF grafting was altered by appropriate reaction recipes to find out the effect of Fe content on various physical properties including fluidity of the HTPB. Density function theory (DFT) calculation showed that the dominating intra-chain interactions over inter-chain owing to the strong interactions between NO<sub>2</sub> of DNB and cyclopentadiene of ferrocene are the driving force for improvement in various physical properties of PVF-grafted-HTPB-DNB. Cyclic voltammetry (CV) measurement showed one electron reversible redox behavior of the grafted PVF polymer chain with slow electron transfer process. Further the mechanical stability, thermal stability and properties of PUs have been studied thoroughly; the results indicated a strong influence of DNB and ferrocene in the chains on the physical properties. All the DNB modified PU membranes displayed exceptionally enhanced flexibility along with much lower T<sub>g</sub> value compared to neat PVF-g-HTPB-PU. The presence of DNB at the chain end of soft segment (SS) causes strong segmental mixing between SS and hard segment (HS) domains which helps in enhancing the elasticity of SS chain by increasing the inter polymer chain distance. Morphology of the hard segment domains formation has been probed by small angle X-ray scattering (SAXS) and further confirmed by FESEM. Burn rate of composite solid propellant made from the HTPB-DNB-g-PVF binder is found to be ~18% larger than the HTPB-DNB.

## 1. Introduction

The global consumption of polyurethane (PU) based materials is growing rapidly for the use in various applications like surface coatings, high performance elastomers, bio-materials, synthetic fibers, automotive suspension bushing, aerospace and so on [1–3]. Recently, metal based PU is the subject of extensive research because of the unique properties owing to the presence of metal in the polymer chain. Significant numbers of reports are now available with complete description of synthesis, properties and applications [4–7]. Ferrocene functionalized metallo-polyol has been used in order to increase burning rate (BR) of composite solid propellant (CSP) [8,9]. However, sublimation while processing, migration and phase separation by

crystallization during storage and sensitivity toward aerial oxidation are the main drawbacks of ferrocene based catalysts to be used in CSP [8–10]. To overcome these problems, several attempts have been made for covalent linking of ferrocene derivatives such as vinyl ferrocene, ferrocenyl silane, acetyl ferrocene etc. onto the polymeric binder such as hydroxyl terminated polybutadiene (HTPB) [11–13]. However, the high viscosity build-up of these ferrocene linked HTPB on storage causes several hurdles such as poor loading, brittleness and mechanical failures of the resulting CSP [14,15]. All the modifications of HTPB reported so far are relied on the grafting of ferrocene derivatives at the pendant vinyl position which alters the microstructure (relative ratio of cis, trans and vinyl content) of HTPB and hence causes the change in the physical properties of HTPB and thus the CSP made from it [16–19].

\* Corresponding author.

E-mail address: [tusharjana@uohyd.ac.in](mailto:tusharjana@uohyd.ac.in) (T. Jana).

<https://doi.org/10.1016/j.eurpolymj.2019.109380>

Received 4 October 2019; Received in revised form 16 November 2019; Accepted 19 November 2019

Available online 21 November 2019

0014-3057/ © 2019 Elsevier Ltd. All rights reserved.

Therefore, it is a challenge to attach ferrocene derivatives to the HTPB backbone by keeping intact the various physical properties almost similar like parent HTPB.

Ferrocenyl groups are known to impart stiffness on the flexible polybutadiene backbone and thus very poor flexibility of the resulting materials was observed with increased Fe content [11,12]. Though many groups had figured out how to improve the mechanical strength (yield strain) of HTPB based PU films [17,20–23] but no efforts were found in literature to improve the flexibility of HTPB based PU films with high Fe content. Very recently, our group has been successful in controlling the viscosity of ferrocene grafted HTPB with improved mechanical properties [24,25]. But further improvement in Fe loading is needed with good control on viscosity and higher mechanical strength of PUs for the use in CSP.

Earlier our group have also explored the influence of terminal functionalization of HTPB on the structure-property (particularly on the mechanical property) relationship of HTPB-PUs using both hydrogen bonding and non-hydrogen bonding functional moieties without altering the inherent properties of parent HTPB [26–29]. We have shown that the nitro functionality containing molecules such as dinitrobenzene (DNB) when attached to terminal position of HTPB is responsible for segmental mixing through hydrogen bonding interactions which in turn improves both tensile strength and elongation of PUs simultaneously [26]. Water dispersible PU (WDPU) developed from HTPB-DNB also displayed superior properties like hydrophobicity, mechanical strength, antibacterial activity etc. [31,32].

These observations, as noted above, motivated us to investigate the effect of enhanced segmental mixing on various physical properties of ferrocenyl based HTPB-DNB-PU owing to the presence of DNB and grafted PVF in the HTPB. Hence in this article, we have modified HTPB by attaching DNB functionality at the terminal position followed by the grafting of poly (vinyl ferrocene) (PVF) at the pendant vinyl bond of HTPB. We expect to get control over viscosity build-up as well as increase in the flexibility of resulting PU films which might happen due to the preponderance of intra-polymer chain interactions between DNB and PVF chains over inter chain interactions throughout the polymer matrix. Very few literature also reported the electrochemistry studies of ferrocenyl based burn rate catalyst [33,34]. To the best of our prior knowledge this work is going to be the first report on the investigation of the redox property of ferrocenyl polymer attached with HTPB matrix. Overall, poly (vinyl ferrocene) grafted HTPB-DNB (PVF-g-HTPB-DNB) with a combination of potential energetic material DNB which is capable to impart some energy to inert HTPB and PVF which can enhance the burn rate property, can be an unique potential binder for rocket propellant in near future.

## 2. Experimental section

### 2.1. Synthesis of poly (vinyl ferrocene) grafted HTPB-DNB (PVF-g-HTPB-DNB)

DNB groups were attached to HTPB terminal position by following terminal functionalization methodology [30] as developed by us earlier. Then vinyl ferrocene (VF) was grafted as PVF chain at the pendant vinyl position of HTPB-DNB by following a clue from the reported literature [35] and modified it substantially. Briefly the procedure was as follows: 3 g (0.536 mmol: calculated based on the molecular weight obtained from GPC analysis) of vacuum dried HTPB-DNB was dissolved in 10 mL of dry toluene in a two neck round bottom flask. 0.051 g (0.268 mmol) of VF was added to this solution in the presence of nitrogen atmosphere. 0.039 g (0.268 mmol) of AIBN was added to the stirring solution and placed in a preheated oil bath at 75 °C under nitrogen atmosphere. The reaction conditions were varied in terms of equivalents of VF with respect to HTPB-DNB and reaction time as detailed in Table 1. The PVF grafted HTPB-DNB (PVF-g-HTPB-DNB) was precipitated by methanol from the reaction mixture. Then the resulting

product was re-dissolved in hexane and precipitated repeatedly using methanol until it was completely free from VF and AIBN. Finally, the obtained product was dried under vacuum at 60 °C for 6 h to remove the last traces of solvent. The brown colored viscous liquid grafted polymer was stored in a closed flask for further use.

### 2.2. Synthesis of polyurethane (PU) from PVF-g-HTPB-DNB

In a two neck round bottom flask, 3 g (0.516 mmol: calculated based on the molecular weight obtained from GPC analysis) of prepolymer was dissolved in 30 mL of anhydrous THF under nitrogen atmosphere. After stirring for 15 min, 0.49 g (2.2 mmol: based on equivalents calculated from hydroxyl value of prepolymer) of isophorone diisocyanate (IPDI) was added and stirred at room temperature for 30 min under continuous nitrogen flow. We kept the –NCO to –OH ratio as 1:1 for all the PU systems. The hydroxyl value of prepolymer was measured to calculate the moles of –OH present in the prepolymer samples. After 30 min, catalytic amount of DBTDL was added as a catalyst and the whole reaction mixture was stirred for another 3 h at room temperature under nitrogen atmosphere. The progress of the reaction was monitored by FT-IR spectroscopic analysis where disappearance of the isocyanate peak at 2270  $\text{cm}^{-1}$  was observed after PU formation. The brown colored viscous polymer solution was then transferred into a clean flat based petri dish pre-coated with silicone releasing agent and the reaction (curing) was continued at 70 °C for 5 days to obtain a free standing PU film.

All details of materials source and the various characterization techniques are described in the [Supplementary material](#).

## 3. Results and discussion

### 3.1. Synthesis of PVF-g-HTPB-DNB

The synthesis of PVF-g-HTPB-DNB was carried out via the free radical reaction pathway with radical initiator AIBN as shown in [Scheme 1](#). At first HTPB-DNB was synthesized by covalently attaching DNB at the terminal carbon of HTPB polymer backbone by using terminal functionalization technique which is already established by our group [30,36,37]. Then free radical grafting of VF was performed onto the pendant vinyl bond of HTPB-DNB backbone as discussed in the experimental section. The mechanism of free radical grafting proceeds in such a way that VF is attached as a growing PVF chains onto HTPB-DNB. We have altered the VF equivalents and the reaction time to tune the viscosities of resulting prepolymer and also to vary the net Fe content in the product. Several parameters such as molecular weight, polydispersity ( $\mathcal{D}$ ), viscosities, Fe content and hydroxyl values of the products were measured and listed in [Table 1](#). All the changes in various physical parameters due to successful grafting of ferrocene functionality onto butadiene backbone are seen. For example, with increased reaction time as well as increased monomer equivalence, both iron content and viscosity of the product increases. The increase in molecular weight is observed along with gradual decrease in hydroxyl value but up to a certain extent. All the parameters show reverse trend beyond 6 equivalent of VF. Ferrocenyl polymer known to cause higher crosslinking in HTPB polymer matrix [4] and as expected higher viscosity build-up during storage was observed with higher amount of iron content in the sample [3,11,38]. In order to optimize the viscosity build-up on storage, we have varied the reaction time up to a certain extent with gradual increase in monomer equivalence ([Table 1](#)). It is important to note that the change in the viscosity values on storage as shown in [Table 1](#) measured after two months of storage. All the PVF-g-HTPB-DNB (abbreviated as FHD) samples shows an increase in viscosity on storage but still within the measurable limit and samples remain fluidic. But in case of PVF-g-HTPB (FH) sample (entry 2 in [Table 1](#)) becomes sticky solid for which viscosity could not be measured. The reason for this will be discussed in the following section

**Table 1**

Variation in reaction conditions and various physical parameters of the all PVF-g-HTPB-DNB (FHD) samples including HTPB-DNB (HD, first entry) and PVF-g-HTPB (FH, 2nd entry).

Sample identity	Reaction time (h)	[VF] (equivalent)	$\bar{M}_n^a$	$\bar{D}^a$	Viscosity (cp) at 30 °C <sup>b</sup>	Viscosity (cp) at 30 °C <sup>c</sup>	Hydroxyl value (mg KOH/g) <sup>d</sup>	Fe content (Wt %) <sup>e</sup>
HD	24	–	5600	2.53	5600	5669	42.5	0.0
FH	17	0.5	6190	2.67	5809	sticky	27.56	0.83
FHD1	4	0.5	5811	2.16	6670	7880	41.78	0.52
FHD2	4	1.5	6332	2.22	5696	10,662	36.33	0.92
FHD3	4	3	8530	1.87	7841	12,892	18.37	2.2
FHD4	4	6	5749	2.6	9883	10,640	23.58	0.88
FHD5	6	0.5	5818	2.55	5100	9620	37.09	0.65
FHD6	6	1.5	6795	2.21	6346	9447	37.42	1.0
FHD7	6	3	6440	2.25	6622	10,913	29.52	1.1
FHD8	6	6	5699	2.45	8292	8957	40.52	0.87
FHD9	17	0.5	6290	2.69	5308	8332	37.9	0.91
FHD10	17	1.5	8143	1.76	7020	12,501	23.05	1.9
FHD11	17	3	7395	2.0	8287	11,530	22.33	1.4
FHD12	17	6	6291	2.8	10,989	13,953	23.62	1.2

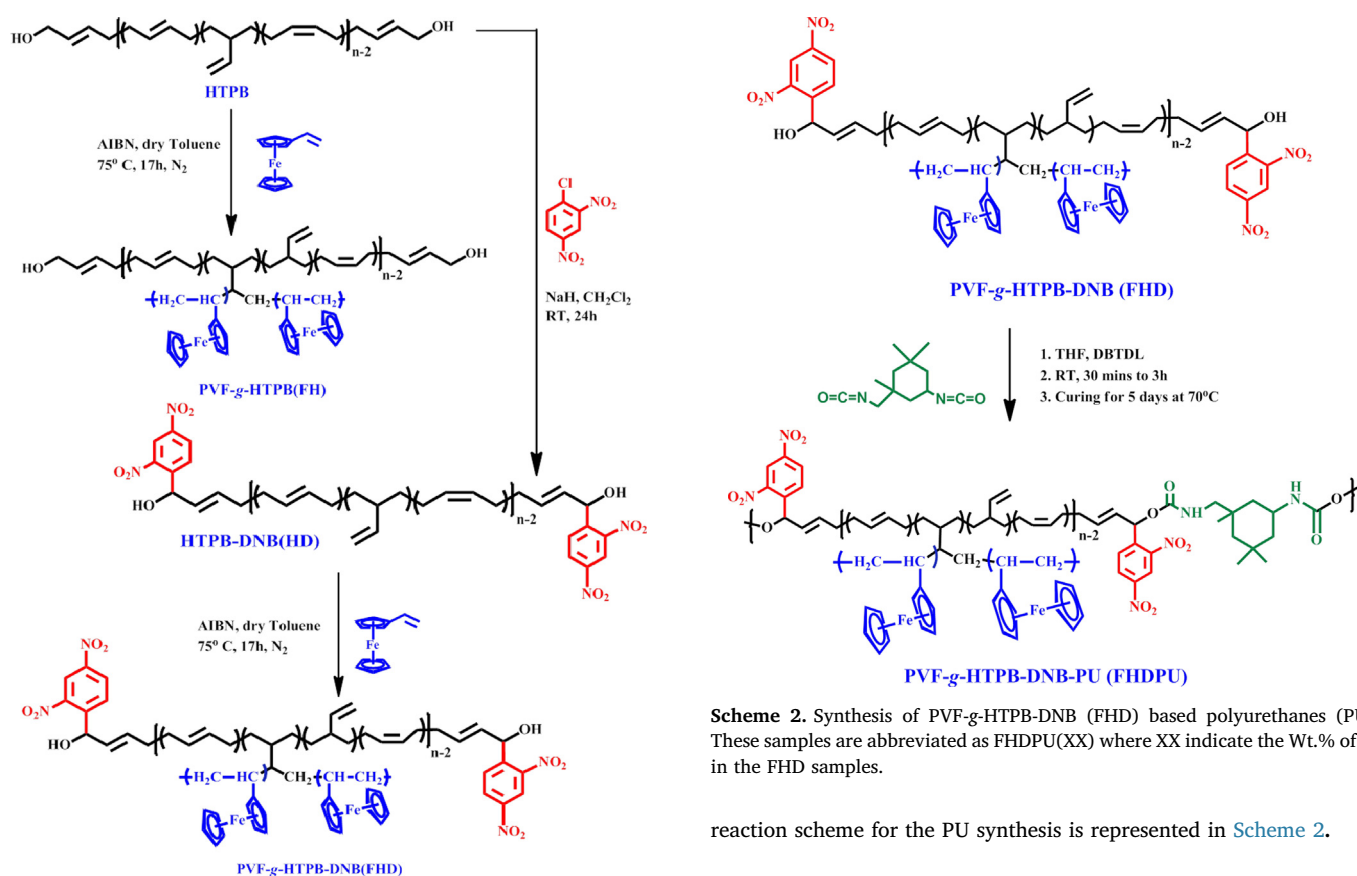
<sup>a</sup> Number average molecular weight ( $\bar{M}_n$ ) and dispersity ( $\bar{D}$ ) are obtained from GPC analysis. All the GPC chromatograms are shown in Supporting Fig. 1.

<sup>b</sup> Measured immediately after preparation.

<sup>c</sup> Measured after two months.

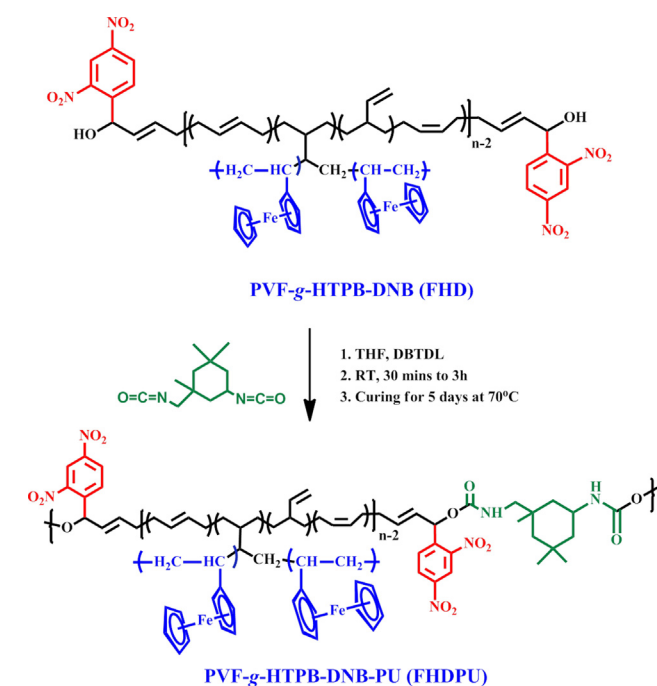
<sup>d</sup> Measured by following acetylation method, which involves the replacement of a hydrogen of hydroxyl group by acetyl group.

<sup>e</sup> Obtained from atomic absorption spectroscopic (AAS) analysis.



Pristine HTPB-DNB (HD), PVF-g-HTPB (FH) and few selected PVF-g-HTPB-DNB (FHD) samples have been used to make PUs with IPDI using DBTDL as catalyst. All together five PU films were prepared in anhydrous THF solvent followed by curing for 5 days at 70 °C keeping the stoichiometric ratio between –NCO/–OH constant and equal to 1:1. The

reaction scheme for the PU synthesis is represented in Scheme 2.



reaction scheme for the PU synthesis is represented in Scheme 2.

### 3.2. Spectroscopic study

The FTIR spectra of HTPB-DNB (HD) and PVF-g-HTPB-DNB (FHD) samples are presented in Fig. 1. The characteristic peaks for HD appeared at 969  $\text{cm}^{-1}$ , 887  $\text{cm}^{-1}$  and 753  $\text{cm}^{-1}$  (Fig. 1A) which correspond to 1,4-trans, 1,2-vinyl and 1,4-cis microstructure of polybutadiene backbone, respectively [30]. After grafting the PVF chains, the 1,2 vinyl peak intensity at 887  $\text{cm}^{-1}$  gradually decreases while a prominent shift has been observed for the peak at 753  $\text{cm}^{-1}$  (1,4 cis) to 699  $\text{cm}^{-1}$  with huge decrease in peak intensity. It is clear from Fig. 1A data that grafting of VF has occurred at the pendant vinyl bond which also mainly affects the cis-microstructure of the DNB modified

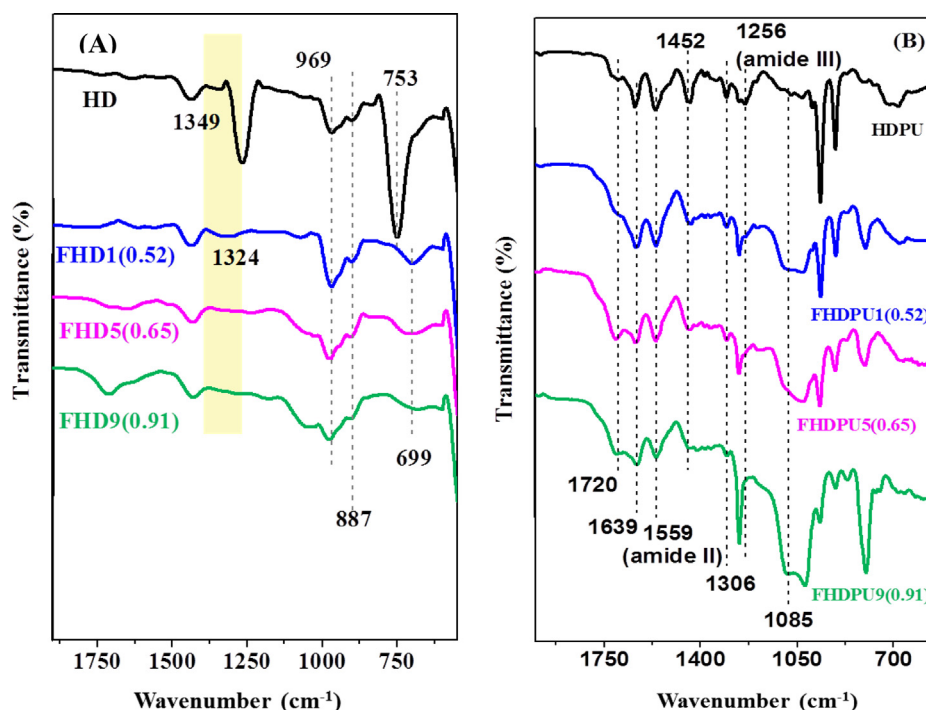


**Fig. 1.** FTIR spectra of (A) HTPB-DNB (HD) and PVF-g-HTPB-DNBs (FHD), (B) HTPB-DNB-PU (HDP) and PVF-g-HTPB-DNB-PUs (FHDPU). Sample names are indicated in the figure. Amount of Fe content in the sample is mentioned in the parenthesis after the sample name.

polybutadiene backbone. Another characteristic peak of HD appears at 1349 cm<sup>-1</sup> which corresponds to asymmetric stretching of -NO<sub>2</sub> of DNB moiety [30] displays peak broadening and shifting to 1324 cm<sup>-1</sup> indicating the involvement of -NO<sub>2</sub> in interactions with grafted PVF. For higher reaction time, most probably because of higher Fe content in the sample FHD9 (0.91) (Fig. 1A) and due to even more interactions the characteristic peak at NO<sub>2</sub> becomes broader and weaker. This interaction between PVF and NO<sub>2</sub> of DNB also affects the OH stretching frequency of FHD which shifts towards higher frequency (3396 to 3412 cm<sup>-1</sup>) (Supplementary Fig. 2A) attributing to the fact that grafted PVF decreases the extent of hydrogen-bonding between -NO<sub>2</sub> and -OH by increasing the interactions between PVF chain with -NO<sub>2</sub>. However, we did not see the similar observations in case of FH sample (data is not shown here) where DNB is not present. These results together indicate that this increased interaction between NO<sub>2</sub> and PVF helps in reducing a substantial increase in viscosity built up in case of FHD. But no such interaction happens in the absence of NO<sub>2</sub> in case of FH which helps to build up very high viscosity on storage and it becomes solid like sticky mass as shown in Table 1. A more detailed discussion on these interactions will be discussed in the forthcoming section.

After curing with IPDI, the characteristic peak of -OH at 3396–3412 cm<sup>-1</sup> completely disappeared and two new bands appeared in principle vibrational region i.e. at 3324–3341 cm<sup>-1</sup> for amine (-NH-) stretching (Supplementary Fig. 2B) and at 1720 cm<sup>-1</sup> for carbonyl peak of the urethane segment (Fig. 1B). The peak at 1639 cm<sup>-1</sup> corresponds to the carbonyl frequency of those which are involved in hydrogen-bonding within the PU matrix and 1085 cm<sup>-1</sup> correspond to C-O-C stretching band for the linkage between -OH and -NCO to form urethane bond [38,53]. A shift for the amide III and amide II band at 1256 cm<sup>-1</sup> and 1559 cm<sup>-1</sup> of HTPB-DNB towards higher wavelength upholds the fact that the hydrogen-bonding between DNB and urethane amide linkage in PU matrix gets disturbed by grafted PVF chain [38]. And the gradual broadness of the characteristic symmetric and asymmetric stretching frequency of -NO<sub>2</sub> at 1452 cm<sup>-1</sup> and 1306 cm<sup>-1</sup> ascertains the gradual increased interaction of -NO<sub>2</sub> with grafted PVF chain [26].

<sup>1</sup>H and <sup>13</sup>C NMR spectra of HD and FHD along with VF in CDCl<sub>3</sub> are

shown in Fig. 2. <sup>1</sup>H NMR spectrum of HD shows resonance peaks at ~7.78, ~8.37 and ~8.75 ppm correspond to aromatic region of DNB moiety which is clearly present in FHD also. Signals appear at ~4–4.4 ppm in case of VF are assigned to the cyclopentadiene ring protons of VF. However, HD also shows the peaks in the similar region. From Fig. 2A, it is clearly visible that due to presence of both ferrocene and DNB, the peak intensity at ~4–4.4 ppm increases prominently in case of FHD with stronger intensities than HD. The other chemical shift regions of HD at  $\delta$  = 2–2.1, 3.4–4.2 and 4.9–5.6 are exactly similar with parent HTPB [26,30] which mainly correspond to the *cis*, *trans*-1,4-unit and vinyl-1,2-unit protons. Some of these peaks are not shown here for better representation. Similarly, <sup>13</sup>C NMR further confirms the structure of the FHD. As shown in Fig. 2B, the resonance peak of ferrocene in case of FHD appears at ~69 ppm which is matching with the resonance peak of ferrocene carbon of VF. Representative peaks for DNB appears at 133.8 and 141 ppm which also present in FHD sample implying the confirmation of grafting of PVF onto HTPB-DNB polymer backbone.

### 3.3. Theoretical study

To understand the origin of the interactions between cyclopentadiene and NO<sub>2</sub> functionality, as evident from IR and NMR studies, we carried out theoretical calculation using density function theory (DFT). Theoretical evaluation using DFT has been performed on two important moieties of polymer chain and these are 2, 4-dinitrobenzene (DNB) and ferrocene, to understand their function in the polybutadiene chain. The physical parameters obtained through DFT calculations using Gaussian package (GAUSSIAN-09) of these two units are shown in Table 2. Ferrocene has approximately zero dipole moment (0.0004 Debye, Table 2) and high polarizability of 33 Bohr<sup>3</sup> which is obtained from DFT calculation. Because of this high polarizability, ferrocene molecule can easily interact with another ferrocene unit through instantaneous induced dipole interactions (London dispersion force). This dispersion force energy can be calculated using the equation.

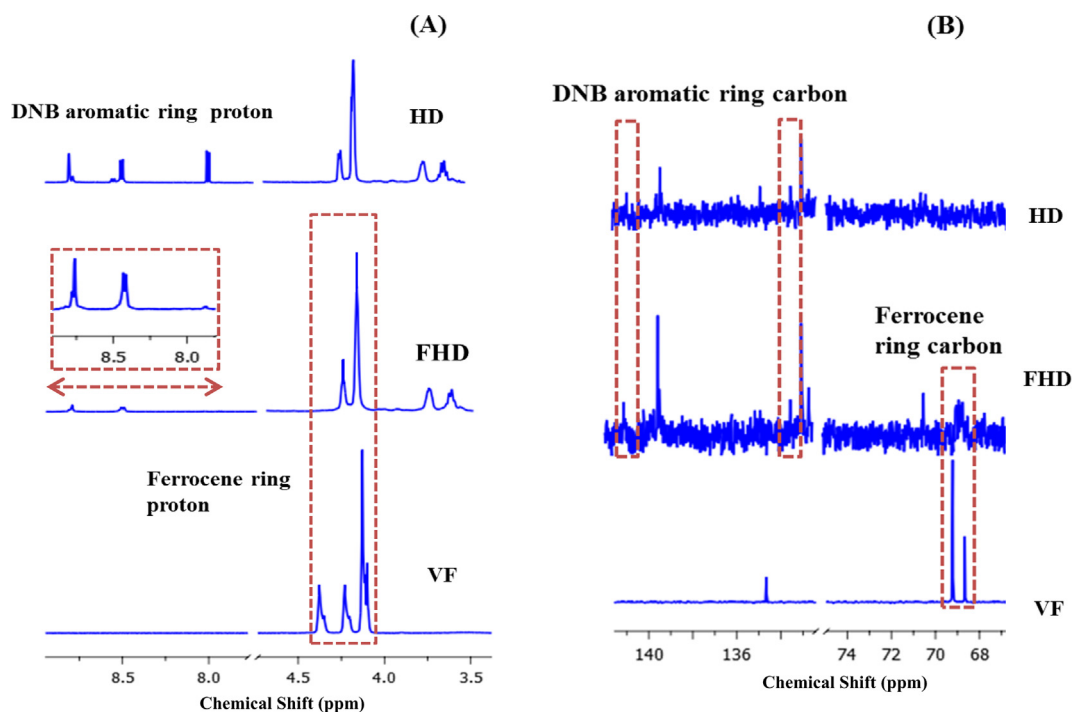


Fig. 2. (A)  $^1\text{H}$  NMR and (B)  $^{13}\text{C}$  NMR spectra of HD, FHD and VF. NMR spectra were recorded using  $\text{CDCl}_3$  as a solvent.

$$E_L = -\frac{3I\alpha^2}{4r^6}$$

where,  $I$  is ionization energy,  $r$  is intermolecular distance between two ferrocene unit which is considered as 0.3 nm and  $\alpha$  is polarizability of ferrocene molecule. Dispersion energy of interaction obtained from the above equation for ferrocene is found to be 17 kJ/mol per pair. Because of this type of strong interactions, ferrocene has strong inter interactions with other ferrocene unit throughout the polymer matrix and results very high viscosity in case of PVF-g-HTPB (FH) sample. The most profound aspect is that these non-covalent interactions between the ferrocene units are quite higher even almost equivalent to hydrogen bonding interactions.

However, once DNB comes into the frame of FH as in FHD, owing to the high electron affinity (201 kJ/mol) and high dipole moment (4.39 Debye) of DNB (Table 2), DNB instantaneously interacts with highly polarizable ferrocene unit available within the same polymer chain (Fig. 3) and indirectly reduces the extent of London dispersion force among ferrocene moieties for further inter interactions. This fact is also supported by the lower ionization value of ferrocene unit (698 kJ/mol, Table 2). Because of lower ionization value ferrocene moiety can easily interact with DNB through its electron cloud as graphically shown in Fig. 3. There will be possibility of both intra and inter interactions throughout the polymer matrix but intra will be dominated as soon as DNB grafted onto the FH backbone (as it is in FHD sample) and will help to minimize the inter polymer chain crosslinking. So, this theoretical calculation clearly certifies that dominance of intra over inter interactions in presence of DNB molecule in the FHD polymer matrix perhaps helps in controlling the viscosity increase. But in absence of DNB as in case of FH, the viscosity increases because of strong inter-chain interactions. In the following section, we will see how this

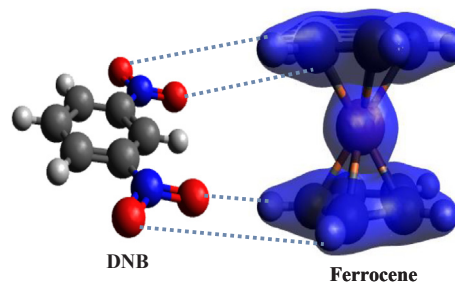


Fig. 3. Graphical view of interactions between DNB and ferrocene ring.

interaction helps in modulating electrochemical properties of FHD.

### 3.4. Electrochemical study

Cyclic voltammetric (CV) waves showing both oxidation and reduction peaks were recorded for monomer (VF), FH and FHD samples with different Fe content in  $\text{CH}_2\text{Cl}_2$  solution. Fig. 4 depicts the current-voltage scan of samples obtained at 20 mV/s scan rate. The cyclic voltammograms show oxidation peaks at 537 mV to 597 mV and reduction peaks at 358 mV to 455 mV. Various electrochemical parameter extracted from the CV waves (Fig. 4) are presented in Table 3 for better clarity. Both anodic current ( $I_{pa}$ ) and cathodic current ( $I_{pc}$ ) values are increasing with increasing Fe content in the FHD samples (Table 3), this observation is consistent with the increase of number of electroactive ferrocene groups per polymer molecule. The difference between anodic and cathodic peak potential ( $\Delta E_p$ ) of FHD samples found to be significantly higher than VF and FH, and increasing with increasing Fe

Table 2

Physical parameters obtained from DFT calculation.

Molecule of interest	Type of calculation	Basis set	Electron affinity (kJ/mol)	Ionization energy (kJ/mol)	Dipole moment (Debye)
DNB	B3LYP/DFT	aug-ccpvdz	201	986	4.39
Ferrocene	B3LYP/DFT	Fe : LANL2DZ C, H: 631 + G*	-16	698	0.0004

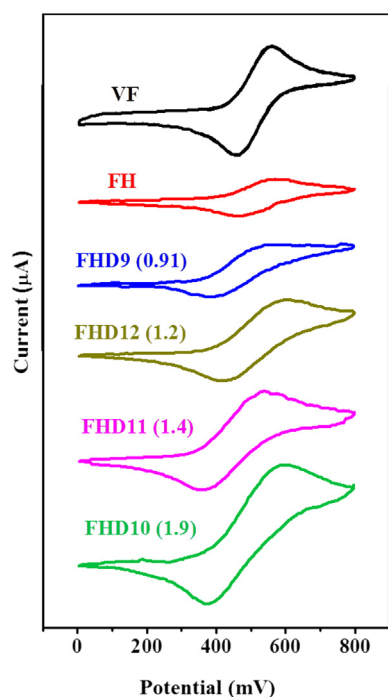


**Fig. 4.** Cyclic voltammograms of PVF-g-HTPB-DNB (FHD) samples along with vinyl ferrocene (VF) and PVF-g-HTPB (FH) in  $\text{CH}_2\text{Cl}_2$  solution. Fe content in the samples is indicated in the parenthesis after sample name. CV were recorded by scanning 800 mV to  $-200$  mV with scan rate of 20 mV/s. 10 mg/ml polymer concentration was used, however for VF 1 mg/ml concentration was used. 10 mmol/L tetrabutylammonium perchlorate was used as supporting electrolyte in  $\text{N}_2$  atmosphere. Pt electrode was used as working electrode and Ag wire was used as reference electrode.

content in FHD samples. This attributes the slow electron transfer process compared to an ideal Nernstian system [39–42] owing to the strong interactions between cyclopentadiene rings and DNB as discussed in earlier sections. Table 3 data also clearly shows that the anodic (oxidation) potential ( $E_{\text{pa}}$ ) values are increasing with Fe content in the FHD indicating that the oxidation becoming more difficult in presence of higher ferrocene content in the backbone of polymer chain. This is because of the fact that the electron cloud of cyclopentadiene is getting pulled by DNB molecules as discussed from our DFT study making the  $\text{Fe}^{+2}$  of ferrocene relatively electron deficient and hence higher  $E_{\text{pa}}$  is obtained. Similarly, we observed the reverse results decreasing cathodic (reduction) potential ( $E_{\text{pc}}$ ) as Fe content increase.

### 3.5. Mechanical properties of polyurethane obtained from FHD

To investigate the influence of DNB, ferrocene and their interactions in the mechanical properties of PVF grafted HTPB-DNB based PUs (FHDPU), few selected FHD samples were converted into PU films and stress-strain profiles were obtained (Fig. 5). Various parameters such as

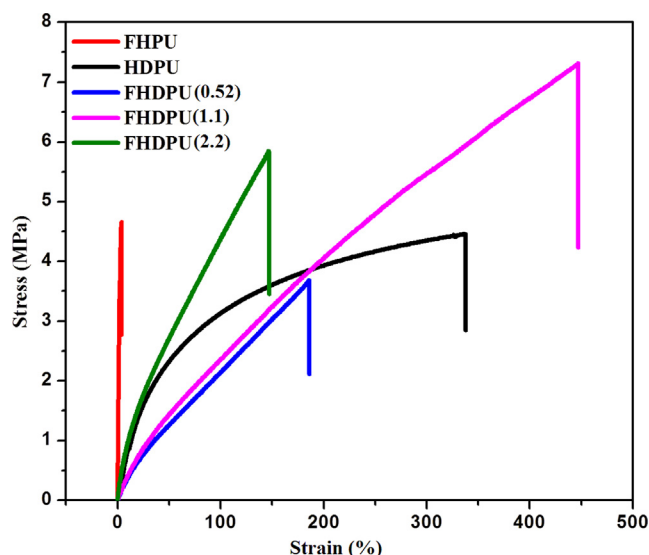


**Fig. 5.** Stress-strain plots of PVF-g-HTPB-PU (FHPU), HTPB-DNB-PU (HDPU) and PVF-g-HTPB-DNB-PUs [FHDPU (0.52–2.2)]. Fe content in the sample is given in the parenthesis after the samples name.

tensile strength ( $\sigma_b$ ), % elongation at break ( $\epsilon_b$ ), Young's modulus ( $E$ ) and toughness were obtained from Fig. 5 are listed in Table 4. The effective cross linking density ( $N$ ) was also estimated and tabulated. Fig. 5 and Table 4 data show clearly that elongation at break ( $\epsilon_b$ ) increased remarkably from FHPU to FHDPU in which DNB is present. This observation can be explained using our DFT calculation results as discussed earlier. The presence of DNB which has very high electron affinity (193 kJ/mol) helps to minimize the inter polymer chain crosslinking through intra interactions of highly polarizable ferrocene unit. These strong intra interactions between DNB and ferrocene help to diminish the effective crosslinking density (Table 4) in the resulting PU matrix and help to obtain more flexible film rather than rigid and hard film. In addition, DNB helps in increasing segmental mixing through extra supramolecular hydrogen bonding between the soft segment (SS) chain end and urethane linkages at the hard segment (HS) region as demonstrated by us earlier [26]. But in case of FHPU, no segmental mixing expected in between polar urethane groups and non-polar PVF chain, rather high rigidity observed throughout the polymer matrix. This fact is attributed to strong intermolecular attraction of hard-to-hard segments as well as higher degree of crosslinking of PVF attached SS chain [4]. Thus the FHPU displays much higher effective crosslinking density to very high Young's modulus (Table 4). But the moment DNB causes segmental mixing through supramolecular hydrogen bonding with urethane groups, crosslinking density also increases at the HS area compared to FHPU. This helps to increase the inter polymer chain distance and reduce the tendency of crosslinking in the polymer matrix which occurs through inter interaction between the grafted PVF. This effect allows the SS to be more flexible to achieve better elongation. Table 4 indicates that with the increase in Fe%, tensile strength

**Table 3**

Electrochemical parameters of the PVF-g-HTPB-DNB (FHD) in  $\text{CH}_2\text{Cl}_2$  solution.

Sample Identity (% of Fe)	$E_{\text{pa}}$ (mV)	$E_{\text{pc}}$ (mV)	$E_{1/2}$ (mV) <sup>a</sup>	$\Delta E_p$ (mV)	$I_{\text{pa}}$ ( $\mu\text{A}$ )	$I_{\text{pc}}$ ( $\mu\text{A}$ )
VF	556 (1.41)	455 (0.47)	505.5 (0.62)	101 (1.7)	$2.8 \times 10^{-1}$	$1.05 \times 10^{-1}$
FH	564 (4.64)	449 (5.66)	506.5 (4.77)	115 (4.02)	$1.23 \times 10^{-1}$	$-1.01 \times 10^{-2}$
FHD9(0.91)	542 (8.01)	373(8.52)	457.5 (8.25)	169 (0.94)	$2.99 \times 10^{-1}$	$1.50 \times 10^{-1}$
FHD12(1.2)	597 (0.94)	410 (1.63)	503.5 (2.35)	187 (2.82)	$3.84 \times 10^{-1}$	$9.19 \times 10^{-2}$
FHD11(1.4)	537 (2.62)	358 (1.63)	447.5 (0.85)	179 (4.03)	$3.83 \times 10^{-1}$	$9.86 \times 10^{-2}$
FHD10(1.9)	594 (3.77)	371 (0.94)	482.5 (1.23)	223 (0.94)	$6.86 \times 10^{-1}$	$1.34 \times 10^{-1}$

Note: All the values are averages of at least three independent measurements. Standard deviations are shown in the parentheses after the data.

<sup>a</sup>  $E_{1/2}$  values are obtained from the  $E_{\text{pa}}$  and  $E_{\text{pc}}$  by averaging their values.

**Table 4**  
Various parameters obtained from tensile study of PVF-g-HTPB-DNB PUs (FHDPUs).

Samples	Tensile strength ( $\sigma_b$ , MPa)	Elongation at break ( $\epsilon_b$ , %)	Toughness (MPa) <sup>a</sup>	Young Modulus (E, MPa) <sup>b</sup>	Effective cross linking (N, m <sup>-3</sup> ) <sup>c</sup>
FHPU	4.626	3.974	12.07	1.89	$1.52 \times 10^{20}$
HDPU	4.44	338.68	1152.53	0.076	$6.11 \times 10^{18}$
FHDPUs(0.52)	3.63	184.9	372.59	0.038	$3.06 \times 10^{18}$
FHDPUs(1.1)	7.285	446.03	1877.84	0.034	$2.73 \times 10^{18}$
FHDPUs(2.2)	5.82	146.88	501.05	0.114	$9.1 \times 10^{18}$

<sup>a</sup> Calculated by integrating the area under stress-strain plot.

<sup>b</sup> Calculated from the slope of the linear portion of the stress-strain plot.

<sup>c</sup> Estimated according to equation  $N = E/(3RT)$ , where E is the Young's modulus, R the gas constant ( $8.314 \text{ J mol}^{-1} \text{ K}^{-1}$ ) and T the absolute temperature in Kelvin.

and elongation at break of FHDPUs increases. As Fe% increases, the intra polymer interactions started dominating over the inter interactions and hence flexibility of SS chain increases. However, at higher Fe% such as in case of FHDPUs (2.2), we observed reverse trend, may be due to inter interactions are dominating after a certain amount of Fe content.

### 3.6. Thermal analysis of the modified PUs

The thermal degradation of most of the samples displays two distinct regions of weight loss (Fig. 6) which is a common feature of this type of PU based on HTPB [26–28]. In the first stage degradation of HDPU started at around-247 °C and reached up to-340 °C with near about 14% weight loss due to the decomposition of urethane linkage in the HS domain, while this range is shifted to lower temperature by-20 °C, i.e. 224 °C to 319 °C for ferrocene modified samples which illustrates the catalytic effect of ferrocene moieties on the thermal decomposition of the hard domains. Although the NCO/OH remains constant for all of the samples, different amount of HS degradation has been observed, most likely because some chain scissions in the SSs simultaneously occurred along with depolycondensation of the urethane linkages at this first degradation stages [43]. The second degradation stage i.e. the major decomposition region for all the HTPB-based PUs started decomposing at ~415 °C up to ~483 °C with more than 80% weight loss for HDPU while for organometallic PUs (FHPU and FHDPUs) it is starting at lower temperature, i.e., 367 °C to 483 °C due to catalytic effect of ferrocene. This second stage mainly is associated with the degradation of polybutadiene segments. Finally, derivative weight% plots i.e. DTG curves (Fig. 6B) explicitly indicate that due to the presence of ferrocene all the FHDPUs and FHPU started decomposing much earlier than parent HDPU especially at the major degradation region. Another aspect also can be analyzed particularly from the DTG curves

(Fig. 6B) i.e., all the char residues after complete decomposition are more for organometallic based PUs rather than HDPU which is an indirect proof of grafting ferrocene moiety onto the polymer matrix.

The degradation pattern obtained from TGA and DTG measurements are in well agreement with the heat change profile obtained from DSC analysis under nitrogen atmosphere (Fig. 7A). The DSC thermograms of FHDPUs show an exothermic peak between 127 and 145 °C while FHPU displays exothermic peak at 135 °C (Fig. 7A). The presence of ferrocene and DNB in the system causes significant changes in DSC profiles. DSC exotherm as obtained is most possibly corresponds to the positive energy balance of endothermic depolymerisation, exothermic cyclization and oxidative crosslinking processes [35,43]. But for HDPU, the exothermic peak appears at about 275 °C only. So it is clear from the data that both DNB and ferrocene has significant influence on the appearance of exothermic peak of FHDPUs system. The DSC evaluations have been further studied to see the phase segregation between HS and SS domains (Fig. 7B). Glass transition temperature of SS domain ( $T_{g-SS}$ ) of all the PUs has been found to be varied from -77 to -66 °C (Fig. 7B, Table 5). As expected in absence of DNB, FHPU displayed the highest  $T_g$  value at -66.46 °C (Table 5). For FHDPUs, the observed  $T_g$  differences of the resulting polyurethanes can be explained in terms of Fe content variation. FHDPUs(0.52), which contains least Fe amount, showed the highest  $T_g$  among all the FHDPUs which is quite obvious because of highest segmental mixing for the lowest amount of Fe in presence of DNB [44]. For higher chain length intra and inter polymer chain interactions playing the key factor to have different  $T_g$  value. Among all, FHDPUs(1.1) showed the lowest  $T_g$  which again because of the preponderance of intra interaction between DNB and PVF chain over inter polymer crosslinking resulting an increase in the mobility of polymer chain soft segments. For further higher Fe content than FHDPUs(1.1), again inter polymer interaction is prevailing than the intra, because of

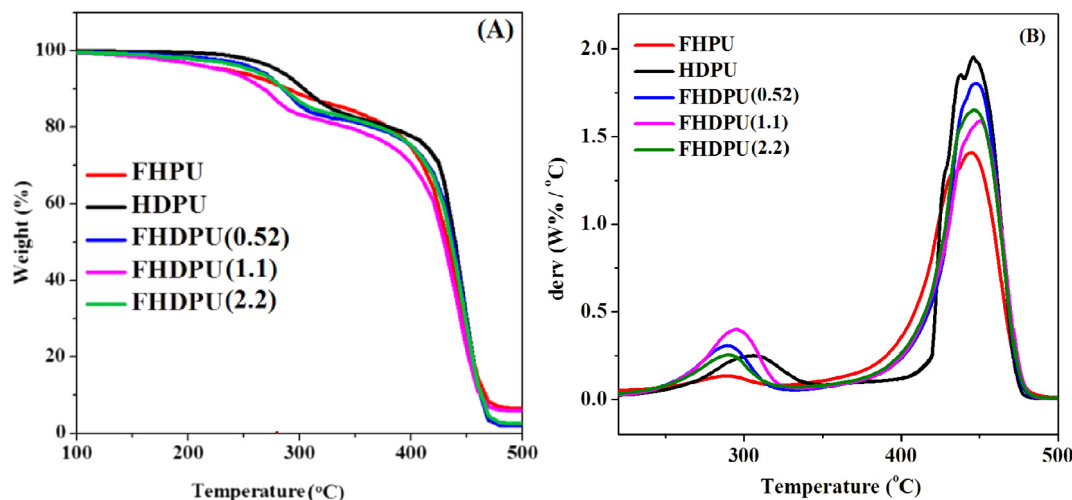


Fig. 6. (A) TGA and (B) DTG curve of FHPUs, HDPU and FHDPUs(0.52–2.2).

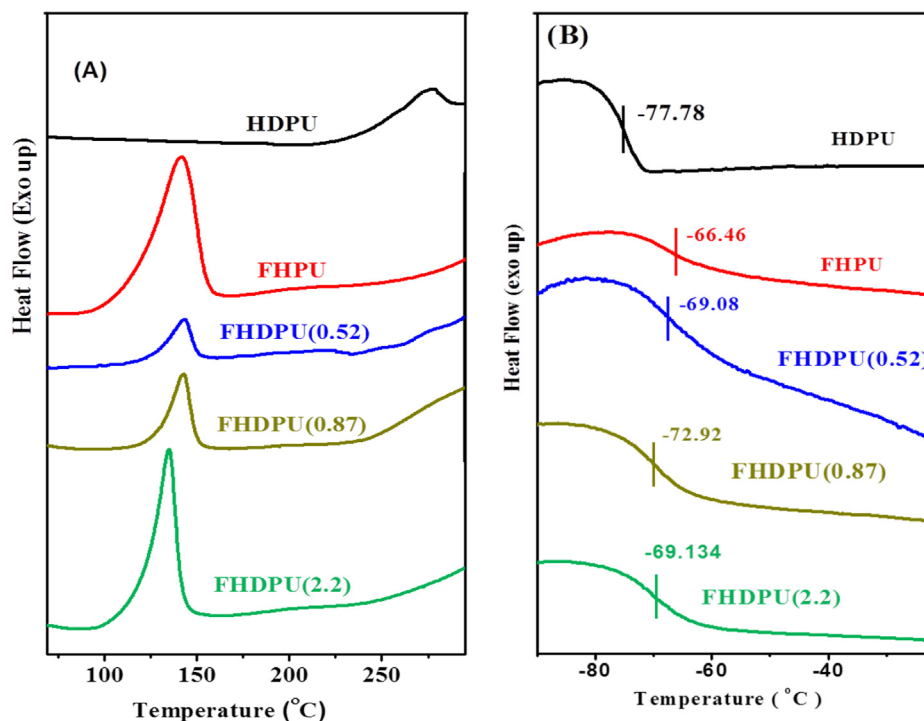


Fig. 7. DSC thermograms of FHPU, HDPUs and FHDPU of their indicated Fe %; in the temperature range: (A) 25–370 °C (B) –100 °C to 25 °C.

Table 5

Glass transition temperature and modulus values of all the PUs from DSC and DMA.

PU samples	$T_{g-ss}$ (°C) from DSC	$T_{g-ss}$ (°C) from $\tan\delta$	$T_{g-HS}$ (°C) from $\tan\delta$	Storage modulus, $E'$ (MPa)
HDPUs	-77.78	-58.5	121	1168
FHPUs	-66.46	-42.9	70.68	1025
FHDPU(0.52)	-69.08	-57.8	138	531
FHDPU(1.1)	-73.96	-57.5	141	3501
FHDPU(2.2)	-69.13	-45.54	17.73	2416

which FHDPU(2.2) possess higher  $T_g$  value than FHDPU(1.1) (Fig. 7B). From DSC thermogram the hard segment  $T_g$  ( $T_{g-HS}$ ) cannot be obtained very clearly and hence we carried out dynamical mechanical analysis (DMA) to find out  $T_{g-HS}$ .

The dependence of  $\tan\delta$  over temperature has been analyzed thoroughly in DMA investigation (Fig. 8A). In maximum cases, two different glass transition regions was observed: the first transition reflects the polymer chain motions of the soft-segment (SS) domain and the second transition corresponds to the motions within hard-segment (HS) units caused by the presence of ferrocenyl groups [4,45]. Fig. 8B and Table 5 data clearly demonstrate that absence of DNB causes too much stiffness in FHPUs film, showing high modulus in the DMA study while the presence of DNB makes FHDPU much more flexible. This result is in agreement with stress-strain plots as discussed in earlier section shows usual trend like earlier report [26]. The soft segment  $T_g$  ( $T_{g-ss}$ ) for HDPUs and FHDPU vary from -58.5 °C to -45.5 °C and hard segment  $T_g$  ( $T_{g-HS}$ ) which originates due to the existence segmental mixing is also obtained from  $\tan\delta$  vs temperature plots and listed in Table 5. The FHDPU (2.2) shows relatively lower  $T_{g-HS}$  may be due to very high degree of segmental mixing. DSC and DMA data (Figs. 7, 8 and Table 5) clearly indicated that both SS and HS  $T_g$  alters as Fe content in the FHDPU changes, attributing significant effect of interactions between cyclopentadienyl ring of ferrocene and  $\text{NO}_2$  group of DNB.

### 3.7. X-ray studies

The structure of samples was explored by investigating WAXD and SAXS techniques. For WAXD analysis, the X-ray patterns of PU samples are compared with bare HTPB-PU for better understanding of difference in the structure in presence of ferrocene functionality along with DNB. HTPB-PU shows a major broad peak at  $2\theta = 19.3^\circ$  and a minor peak at  $42^\circ$  reflecting the amorphous nature of the general polybutadiene based polyurethanes [28]. HDPUs exhibits the presence of crystalline peaks at  $2\theta = 13.89^\circ$ ,  $16.68^\circ$  and  $25.11^\circ$  (Supplementary Fig. 3) which is in well agreement with reported in literature [26] as all other PUs show almost identical diffraction pattern like HDPUs exhibiting crystalline peaks at  $2\theta = 13.89^\circ$ ,  $16.68^\circ$ ,  $25.11^\circ$  and broad amorphous peaks at  $19.3^\circ$  and  $42^\circ$ . The crystalline peaks vary only in intensity, may be due to strong interactions between HS and SS through intra as well as inter polymer chain crosslinking. Among FHDPU, the differences in crystalline peak intensity clearly indicate that varying amount of Fe percentage makes difference in polymer interaction pattern.

Small angle X-ray (SAXS) measurements were carried out on all samples of HDPUs, FHPUs and FHDPU. Figs. 9 and 10 shows typical SAXS profiles displayed on log-log scale for HDPUs and FHDPU (0.52), respectively. For other samples, the shape of curves is similar to anyone of these two.

The SAXS profiles of HDPUs, FHDPU (1.1) and FHDPU (2.2) show linear variation in low-Q, high-Q regions and a broad hump in the middle-Q region as shown in Fig. 9. The linear behavior indicates power-law ( $Q^{-\alpha}$ ) variation of intensity  $I(Q)$  where the value of the exponent ( $\alpha$ ) indicates structural morphology of scatterers. If the linear variation spans over more than a decade of Q, a non-integer value of  $\alpha$  suggests fractal nature; mass fractals of dimension  $D_m (= \alpha)$  if  $\alpha < 3$  and a surface fractal with rough surface if  $3 < \alpha < 4$  [46]. For scattering from smooth surface  $\alpha$  will be 4, following Porod's law. Extensive structural studies [25,28,47,48] showed that PU undergoes micro-phase segregation to hard and soft segments during preparation. If the hard segment domains are spatially correlated, a peak will be visible in the SAXS data.

Thus, broad maximum in the mid-Q region suggests correlation

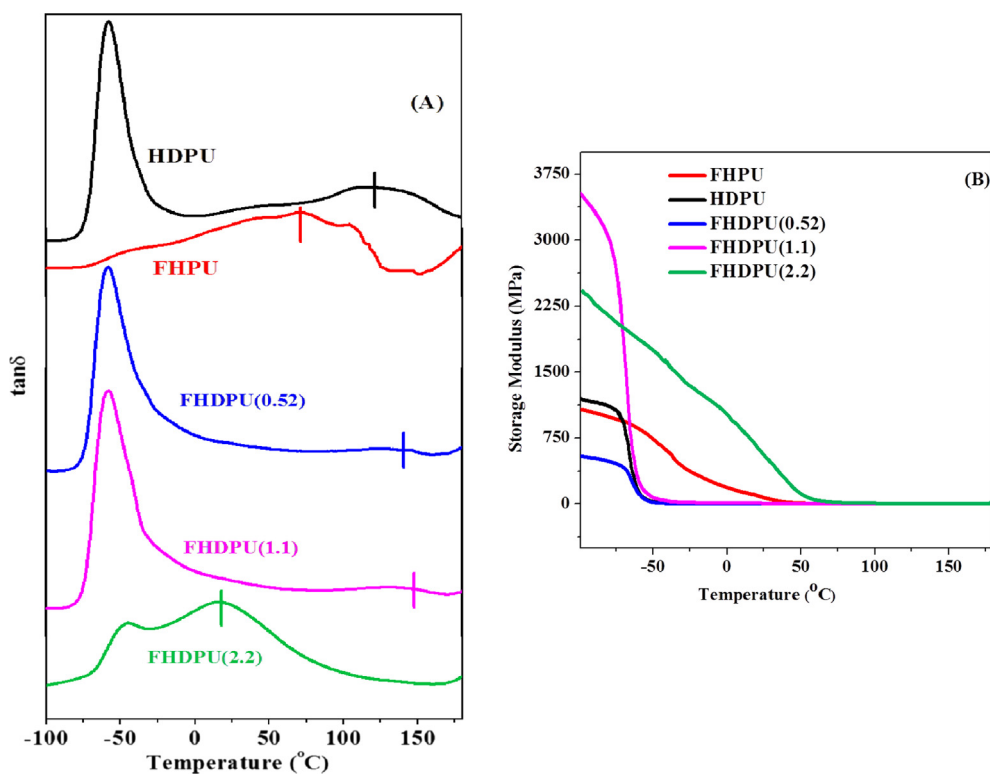


Fig. 8. (A)  $\tan\delta$  vs temperature (B) Storage modulus vs temperature plots of FHPU, HDPU and FHDPU of their indicated Fe content. Plots in case of  $\tan\delta$  vs temperature are shifted vertically for better clarification.

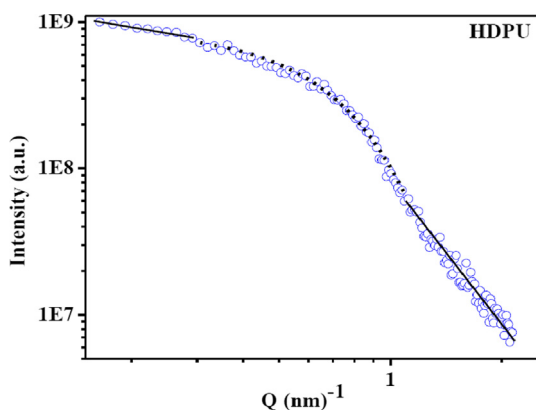


Fig. 9. Small angle X-ray scattering profile of HDPU. Solid line is representation of power-law. Dashed line is fit to the data.

between the positions of domains existing in the polymer matrix. The data in this region is fitted well to the Guinier equation [49,50].

$$I = I_0 e^{-R_g^2 \frac{q^2}{3}}$$

where  $R_g$  is the radius of gyration of the domains. The radius of the domains is found to vary between 2.7 and 3.3 nm. The average distance ( $d$ ) between domains can be found from the peak position ( $Q_m$ ) and is in the range 8–10 nm with minimum value for FHDPU (1.4). The slope of SAXS data in the High- $Q$  region varies between 2.8 and 2.9, suggesting that domains are made of compact, highly dense mass with fractal morphology.

The low- $Q$  region has limited number of data points; hence details on the structure cannot be obtained, although the slope value in the range 1.1–1.3 indicates the presence of loosely bound polymer aggregates. It is known [51,52] that the hard segment domains self-organize to form aggregates of  $\mu\text{m}$  size due to inter molecular hydrogen

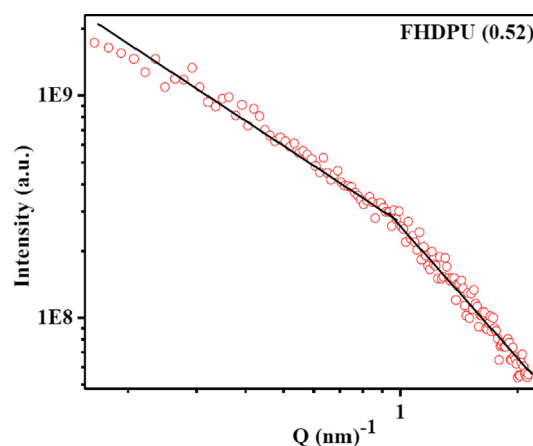
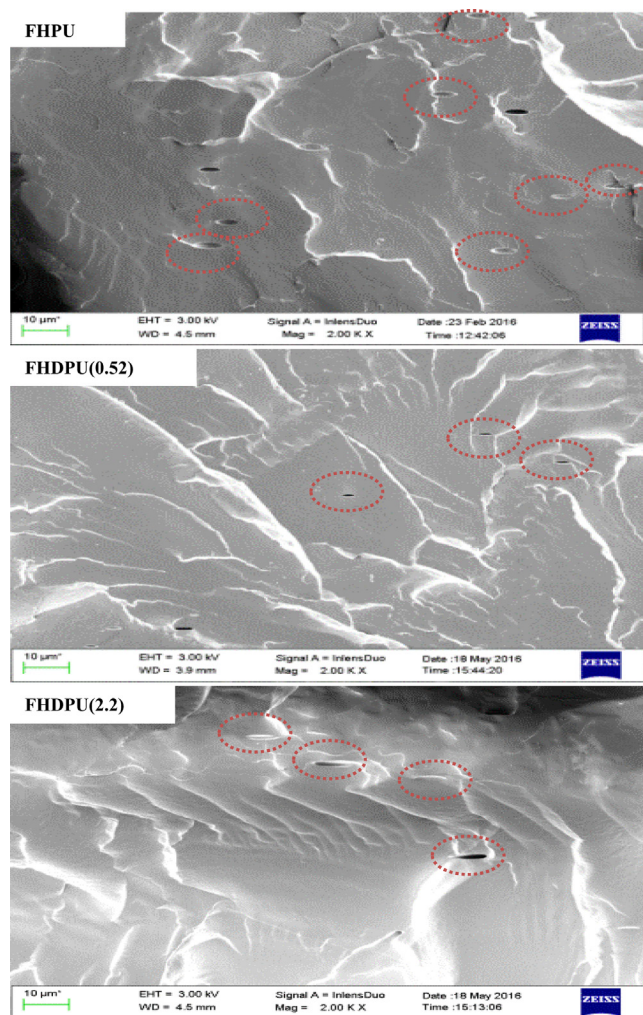


Fig. 10. SAXS profile of samples FHDPU (0.52). Solid lines are representation of power-law.

bonding. Thus, it is possible that SAXS profiles at low- $Q$  region arise from aggregation of HS formed during the preparation of samples. Since the upper  $Q$ -limit of the mass fractal is well below the  $Q$ -range of study, the average size of the aggregates cannot be obtained from SAXS data, though it will be  $> 40$  nm. On the hand for the samples FHPU, FHDPU (0.52), the SAXS profiles vary linearly with change of slope at a  $Q$  as showed in Fig. 10. The power-law exponent in the low- $Q$  region varies between 1.1 and 1.3 suggesting that the samples consist loose compact polymer rich regions or aggregates of HS domains with mass fractal structure. In the high- $Q$  region, representing the structure on smaller length scale, the slope of the line varies between 1.7 and 2.3. This indicates the presence of smaller dense crystallites or HS domains. From the crossover point of two lines, the average radius of the domains is found to be in the range 3.6–4.1 nm.

Comparing the two set of samples, two prominent differences can be



**Fig. 11.** FESEM images of the cross-section of cryo-fractured PU films: FHPU, FHDPU(0.52) and FHDPU(2.2).

noticed. The domains formed in Fig. 10 are not spatially correlated, less compact and marginally larger whereas in Fig. 9, they are correlated and highly compact.

### 3.8. Morphological study

The formation of HSD as confirmed by SAXS study also appears in morphology when the cross-section of the cryo-fractured PU films studied by FESEM analysis (Fig. 11). The fibrous-assembly morphology which are crossed and entangled with each other has been observed for HDPU (not shown here) which is well accord with our earlier report [36]. In other cases, we can clearly see that the phase segregated polymer rich regions with compact mass fractal appear like solid elliptic sphere (shown by the dotted red line in the images). This again may be attributed to preponderance of DNB to PVF intra interaction over inter polymer chain interactions. Another aspect also can be observed in terms of packing nature, except for FHPU all other ferrocene modified PU has got nice well-ordered packing pattern, this may be because of presence of DNB. Ferrocene containing polymer in presence of DNB gets packed in a particular manner giving nice layered kind morphology which is totally absent for FHPU. And as expected with increase in Fe content segregated domain size also increases.

### 3.9. Burn rate analysis of composite solid propellants (CSPs)

Burn rate measurements of CSP made from the binders HD and

**Table 6**

Burn rate and pressure index of CSPs made from HTPB-DNB (HD) and HTPB-DNB-g-PVF (FHD) binders.

CSP	Binder Used	Fe (Wt%) in Binder	Burn rate (mm/s) at 40 bar	Pressure index
P1	HD	0.00	10.08	0.58
P2	FHD2	0.92	11.95	0.33

FHD2 (one representative sample of HTPB-DNB-g-PVF) were performed using a standard Crawford bomb in conjunction with a pressure transducer. The detail experimental procedure is given in the [supplementary materials](#). Table 6 data summarizes the burn rate results of the CSPs. The burn rate of the CSP (P2) made using the FHD binder is found to be ~18% higher than the CSP (P1) of HD binder. It is also to be noted that the pressure index value of P2 CSP is quite significantly lower than the P1. These above observations prove that the CSP made from the PVF grafted HD has higher burn rate than pristine HD and is quite stable with less sensitivity [24].

## 4. Conclusion

A series of poly (vinyl ferrocene) grafted dinitrobenzene containing polybutadiene (PVF-g-HTPB-DNB) have been prepared successfully and all their physical properties have been characterized and correlated with PVF-g-HTPB as well as bare HTPB-DNB. In every case, we have been able to incorporate good amount of Fe with good control in viscosity having high storage capacity and hence can be claimed to be a potential burn rate modifier binder for composite solid propellant. The reversible redox property of grafted PVF over HTPB polymer matrix has been thoroughly analyzed which may explore a new direction of this polymer. Further, we have made polyurethane samples by using PVF-g-HTPB-DNB as soft segments and IPDI as hard segments with constant NCO/OH ratio. In comparison with PVF-g-HTPB-PU, all the PVF-g-HTPB-DNB-PU displayed an outstanding elasticity, attributed to inclusion of DNB into the polymer matrix. DNB caused a supramolecular hydrogen bonding with HS at the SS chain end. That helped to increase the inter polymer chain distance and thus SS flexibility increases. Based on DSC and DMA study, PVF-g-HTPB-DNB-PU possessed lower glass transition temperature than of PVF-g-HTPB-PU. WAXD and SAXS analysis indicated the presence of small dense aggregates or crystallites which appeared because of phase segregation. This phase segregation in PU film had been further confirmed by the appearance of round to ellipsoid shaped hard segment domains in FESEM. Based on the burn rate data as well as other characterization data, PVF-g-HTPB-DNB-PU expected to be used as binder cum burn rate catalyst in composite solid propellant.

## 5. Author statement

All authors contributed equally and jointly.

## Declaration of Competing Interest

We declare that we have no conflict of interest.

## Acknowledgment

MD acknowledges Department of Science and Technology for INSPIRE fellowship during this period. We also thankful to UGC-CAS, PURSE, UPE programme of UoH for financial support. We thank Mrs. Chandrika at ICAR for helping us to determine the Fe content through AAS technique. We thank Prof. S. Pal for the helpful discussions on cyclic voltammetry data. Also, we would like to sincerely thank Prof. S. Mahapatra for allowing us to carry out DFT calculation in his

laboratory. We sincerely acknowledge the help and support of Prof. P. A. Ramakrishna, Department of Aerospace Engineering, Indian Institute of Technology Madras, Chennai for providing the laboratory facility to measure the burn rate of propellants.

## Appendix A. Supplementary material

Supplementary data to this article can be found online at <https://doi.org/10.1016/j.eurpolymj.2019.109380>.

## References

- [1] D. Randall, S. Lee, *The Polyurethanes Book*, John Wiley & Sons, London, 2003.
- [2] C. Priscariu, *Polyurethanes Elastomers. From Morphology to Mechanical Aspects*, Springer-Verlag, Wien, New York, 2011.
- [3] B. Lucio, J.L.D.L. Fuente, Kinetic and chemorheological modelling of the polymerization of 2,4-Toluenediisocyanate and ferrocene-functionalized hydroxyl-terminated polybutadiene, *Polymer* 140 (2018) 290–303.
- [4] B. Lucio, J.L.D.L. Fuente, L.M. Cerrada, Characterization of phase structures of novel metallo-polyurethanes, *Macromol. Chem. Phys.* 216 (2015) 2048–2060.
- [5] G.R. Whittell, I. Manners, *Metallopolymers: new multifunctional materials*, Adv. Mater. 19 (2007) 3439–3468.
- [6] J.C. Eloi, L. Chabanne, G.R. Whittell, I. Manners, *Metallopolymers with emerging applications*, Mater. Today 11 (2008) 28–36.
- [7] A.S.A.E. Aziz, E.A. Strohm, Transition metal-containing macromolecules: En route to new functional materials, *Polymer* 53 (2012) 4879–49211.
- [8] R. Tong, Y. Zhao, L. Wang, H. Yu, F. Ren, M. Saleem, W.A. Amer, Recent research progress in the synthesis and properties of burning rate catalysts based on ferrocene-containing polymers and derivatives, *J. Organomet. Chem.* 755 (2014) 16–32.
- [9] J. Gao, L. Wang, H. Yu, A. Xiao, W. Ding, Recent research progress in burning rate catalysts, *Propellants Explos. Protech.* 36 (2011) 404–409.
- [10] W. Zhou, L. Wang, H. Yu, R. Tong, Q. Chen, J. Wang, X. Yang, Z. Abdin, M. Saleem, Progress on the synthesis and catalytic and anti-migration properties of ferrocene-based burning rate catalysts, *Appl. Organometal. Chem.* 30 (2016) 796–805.
- [11] K. Subramanian, K.S. Sastri, Synthesis and characterization of iron carbonyl-modified hydroxyl-terminated polybutadiene: a catalyst-bound propellant binder for burn-rate augmentation, *J. Appl. Polym. Sci.* 90 (2003) 2813–2823.
- [12] A. Unver, N. Dilsiz, M. Volkan, G. Akovali, Investigation of acetyl ferrocene migration from hydroxyl-terminated polybutadiene based elastomers by means of ultraviolet-visible and atomic absorption spectroscopic techniques, *J. Appl. Polym. Sci.* 96 (2005) 1654–1661.
- [13] B.S. Cho, S.T. Noh, Thermal properties of polyurethane binder with 2-(ferrocenyl-propyl)dimethylsilane-grafted hydroxyl-terminated polybutadiene, *J. Appl. Polym. Sci.* 121 (2011) 3560–3568.
- [14] K. Fujimura, A. Miyake, Effect of the particle size and specific surface area of ferric oxide catalyst on the burning rate of AP/HTPB solid propellant, *Sci. Technol. Energetic Mater.* 71 (2010) 65–69.
- [15] G.M. Gore, A.N. Nazare, C.N. Divekar, S.K. Hait, S.N. Asthana, Studies non-aluminized high burning rate AP-composite propellants, *J. Energetic Mater.* 22 (2004) 151–169.
- [16] Q. Zhou, S. Jie, B.G. Li, Preparation of hydroxyl-terminated polybutadiene with high cis-1,4 content, *Ind. Eng. Chem. Res.* 53 (2014) 17884–17893.
- [17] Z. Cao, Q. Zhou, S. Jie, B.G. Li, High cis-1,4 hydroxyl-terminated polybutadiene-based polyurethanes with extremely low glass transition temperature and excellent mechanical properties, *Ind. Eng. Chem. Res.* 55 (2016) 1582–1589.
- [18] Q. Zhou, B.G. Li, S. Jie, N. Zheng, Solvent effect on cis-1,4-specific polymerization of 1,3-butadiene with  $\text{CoCl}_2(\text{PRPh}_2)_2$ -EASC catalytic systems, *Catal. Sci. Technol.* 4 (2014) 773–779.
- [19] Q. Zhou, S. Jie, B.G. Li, Facile synthesis of novel HTPBs and EHTPBs with high cis-1,4 content and extremely low glass transition temperature, *Polymer* 67 (2015) 208–215.
- [20] J.P. Santerre, J.L. Brash, Physical properties of nonionic and ionic segmented polyurethanes: effect of sulfonate, carboxylate, and quaternary ammonium ions in the hard segment, *Ind. Eng. Chem. Res.* 36 (1997) 1352–1359.
- [21] S. Sarkar, B. Adhikari, Synthesis and characterization of lignin-HTPB copolyurethane, *Eur. Polym. J.* 37 (2001) 1391–1401.
- [22] S.L. Huang, P.H. Chang, M.H. Tsai, H.C. Chang, Properties and pervaporation performances of crosslinked HTPB-based polyurethane membranes, *Sep. Purif. Technol.* 56 (2007) 63–70.
- [23] M. Amrollahi, G.M.M. Sadeghi, Y. Kashcooli, Investigation of novel polyurethane elastomeric networks based on polybutadiene-ol/polypropyleneoxide mixture and their structure-properties relationship, *Mater. Design.* 32 (2011) 3933–3941.
- [24] B.N. Rao, K. Malkappa, N. Kumar, T. Jana, Ferrocene grafted hydroxyl terminated polybutadiene: a binder for propellant with improved burn rate, *Polymer* 163 (2019) 162–170.
- [25] B.N. Rao, P.U. Sastry, T. Jana, Structure-property relationships of ferrocene functionalized segmented polyurethane, *Eur. Polym. J.* 115 (2019) 201–211.
- [26] K. Malkappa, T. Jana, Simultaneous improvement of tensile strength and elongation an unprecedented observation in the case of hydroxyl terminated polybutadiene polyurethanes, *Ind. Eng. Chem. Res.* 52 (2013) 12887–12896.
- [27] B.K. Sikder, T. Jana, Effect of solvent and functionality on the physical properties of hydroxyl-terminated polybutadiene (HTPB)-based polyurethane, *ACS Omega* 3 (2018) 3004–3013.
- [28] B.N. Rao, P.J.P. Yadav, K. Malkappa, T. Jana, P.U. Sastry, Triazine functionalized hydroxyl terminated polybutadiene polyurethane: Influence of triazine structure, *Polymer* 77 (2015) 323–333.
- [29] K.R. Kunduru, B.N. Rao, T. Jana, Self-assembly in functionalized butadiene based polyurethanes, *Macromol. Symp.* 382 (1800090) (2018) 1–6.
- [30] R.M. Shankar, T.K. Roy, T. Jana, Terminal functionalized hydroxyl-terminated polybutadiene: an energetic binder for propellant, *J. Appl. Polym. Sci.* 114 (2009) 732–741.
- [31] K. Malkappa, B.N. Rao, T. Jana, Functionalized polybutadiene diol based hydrophobic, water dispersible polyurethane nanocomposites: Role of organo-clay structure, *Polymer* 99 (2016) 404–416.
- [32] K. Malkappa, T. Jana, Hydrophobic, water-dispersible polyurethane: role of polybutadiene diol structure, *Ind. Eng. Chem. Res.* 54 (2015) 7423–7435.
- [33] F. Xiao, X. Sun, X. Wu, J. Zhao, Y. Luo, Synthesis and characterization of ferrocenyl-functionalized polyester dendrimers and catalytic performance for thermal decomposition of ammonium perchlorate, *J. Organomet. Chem.* 713 (2012) 96–103.
- [34] Z. Cheng, G. Zhang, X. Fan, F. Bi, F. Zhao, W. Zhang, Z. Gao, Synthesis, characterization, migration and catalytic effects of energetic ionic ferrocene compounds on thermal decomposition of main components of solid propellants, *Inorgan. Chim. Acta* 421 (2014) 191–199.
- [35] K. Subramanian, Synthesis and characterization of poly(vinyl ferrocene) grafted hydroxyl-terminated poly(butadiene): a propellant binder with a built-in burn-rate catalyst, *J. Polym. Sci. A.* 37 (1999) 4090–4099.
- [36] R.M. Shankar, S. Saha, K.S. Meera, T. Jana, Functionalization of hydroxyl terminated polybutadiene with biologically active fluorescent molecule, *Bull. Mater. Sci.* 32 (2009) 507–514.
- [37] R.M. Sankar, T.K. Roy, T. Jana, Functionalization of terminal carbon atoms of hydroxyl terminated polybutadiene by polyazido nitrogen rich molecules, *Bull. Mater. Sci.* 34 (2011) 745–754.
- [38] B. Lucio, J.L.D.L. Fuente, Rheokinetic analysis on the formation of metallo-polyurethanes based on hydroxyl-terminated polybutadiene, *Eur. Polym. J.* 50 (2014) 117–126.
- [39] Y. Tang, X. Zeng, Poly(vinyl ferrocene) redox behavior in ionic liquids, *J. Electrochem. Soc.* 155 (2008) F82–F90.
- [40] A.L. Crumbliss, D. Cooke, J. Castillio, P.W. Neilson, Redox properties of phosphazene polymers with pendant ferrocene groups, *Inorg. Chem.* 32 (1993) 6088–6094.
- [41] D.C. Kraitter, P.W. Neilson, C. Zhang, A.L. Crumbliss, Synthesis and redox characterization of phosphazene terpolymers with pendant ferrocene groups, *Macromolecules* 45 (2012) 3658–3668.
- [42] B.M. Upton, R.M. Gipson, S. Duhovic, B.R. Lydon, N.M. Matsumoto, H.D. Maynard, P.L. Diaconescu, Synthesis of ferrocene-functionalized monomers for biodegradable polymer formation, *Inorg. Chem. Front.* 1 (2014) 271–277.
- [43] B. Lucio, J.L.D.L. Fuente, Structural and thermal degradation properties of novel metallocenepolyurethanes, *Polym. Degrad. Stab.* 136 (2017) 39–47.
- [44] S. Alibeik, A.S. Rizkalla, K. Mequanint, The effect of thiolation on the mechanical and protein adsorption properties of polyurethanes, *Eur. Polym. J.* 43 (2007) 1415–1427.
- [45] T. Seyidoglu, M.A. Bohn, Characterization of aging behavior of butacene based composite propellants by loss factor curves, *Propellants Explos. Pyrotech.* 42 (2017) 1–13.
- [46] P.W. Schmidt, Small-angle scattering studies of disordered, porous and fractal systems, *J. Appl. Cryst.* 24 (1991) 414–435.
- [47] S.L. Chang, T.L. Yu, C.C. Huang, W.C. Chen, K. Linliu, T.L. Lin, Effect of polyester side-chains on the phase segregation of polyurethanes using small-angle X-ray scattering, *Polymer* 39 (1998) 3479–3489.
- [48] J.T. Koberstein, A.F. Galambos, L.M. Leung, Compression-molded polyurethane block copolymers. 1. Microdomain morphology and thermomechanical properties, *Macromolecules* 25 (1992) 6195–6204.
- [49] A. Guinier, G. Fournet, *Small Angle Scattering of X-rays*, Wiley, New York, 1955.
- [50] O. Glatter, O. Kratky, *Small Angle X-ray Scattering*, Academic, London, 1982.
- [51] M. Song, H.S. Xia, K.J. Yao, D.J. Hourston, A study on phase morphology and surface properties of polyurethane/organoclay nanocomposite, *Eur. Polym. J.* 41 (2005) 259–266.
- [52] A. Aneja, G.L. Wilkess, A systematic series of 'model' PTMO based segmented polyurethanes reinvestigated using atomic force microscopy, *Polymer* 44 (2003) 7221–7228.
- [53] J. Bandekar, S. Klima, FT-IR spectroscopic studies of polyurethanes Part I. Bonding between urethane C-O-C groups and the NH Groups, *J. Mol. Struct.* 263 (1991) 45–57.